Journal of Hazardous Materials 438 (2022) 129412

Contents lists available at ScienceDirect

Journal of Hazardous Materials

journal homepage: www.elsevier.com/locate/jhazmat

Tuning the sensing responses towards room-temperature hypersensitive methanol gas sensor using exfoliated graphene-enhanced ZnO quantum dot nanostructures

Ji Young Park [a], Yeonsu Kwak [b], Hyo-Ryoung Lim [c], Si-Woo Park [a], Min Seob Lim [a], Hong-Baek Cho [a], Nosang Vincent Myung [d], Yong-Ho Choa [a,*]

[a] Department of Materials Science and Chemical Engineering, Hanyang University, Ansan 15588, Republic of Korea
[b] Department of Chemical and Biomolecular Engineering, University of Delaware, Newark 19716, United States
[c] Major of Human Biocovergence, Division of Smart Healthcare, College of Information Technology and Convergence, Pukyong National University, Busan 48513, Republic of Korea
[d] Department of Chemical and Biomolecular Engineering, University of Notre Dame, Notre Dame 46556, United States

HIGHLIGHTS

- A capacitive methanol sensor was designed using exfoliated graphene and ZnO quantum dots on anodic aluminum oxide.
- Vertical electrode configuration enabled faster sensing response than horizontal one.
- ZnO enhanced the methanol uptake of the sensor by enhancing UV absorption at 100 kHz.
- A 2-ppb level of LOD methanol detection was achieved at ambient conditions under UV.
- Sensor performance was reproducible and stable in 60% humidity conditions.

GRAPHICAL ABSTRACT

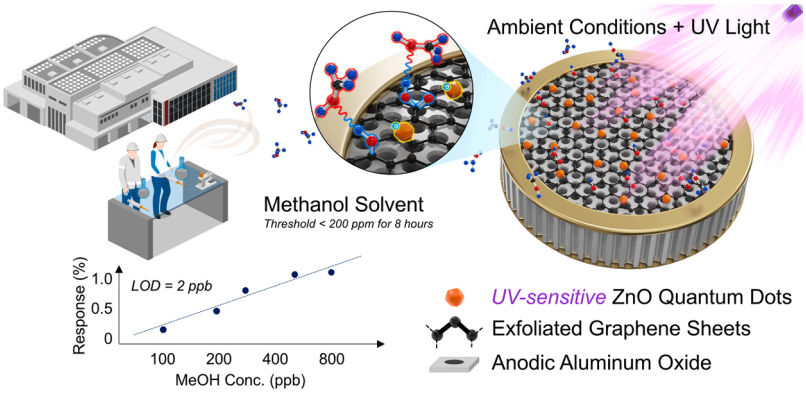

ARTICLE INFO

Editor: John D Atkinson

Keywords:
Capacitive gas sensor
Methanol sensor
Exfoliated graphene sheets
ZnO quantum dot

ABSTRACT

A suitable and non-invasive methanol sensor workable in ambient temperature conditions with a high response has gained wide interest to prevent detrimental consequences for industrial workers from its low-level intoxication. In this work, we present a tunable and highly responsive ppb-level methanol gas sensor device working at room temperature via a bottom-up synthetic approach using exfoliated graphene sheet (EGs) and ZnO quantum dots (QDs) on an aluminum anodic oxide (AAO) template. It is verified that EGs-supported AAO with a vertical electrode configuration enabled high and fast-responsive methanol sensing. Moreover, the hydroxyl and carboxyl groups of the high surface area EGs and ZnO QDs with a 3.37 eV bandgap efficiently absorbing UV light led to 56 times high response due to the enhanced polarization on the sensor surface compared to non-UV-radiated EGs/AAO at 800 ppb of methanol. The optimal resonance frequency of methanol is determined to be 100 kHz, which could detect methanol with high response of 2.65% at 100 ppm. The limit of detection (LOD) concentration is

* Corresponding author.
E-mail address: choa15@hanyang.ac.kr (Y.-H. Choa).

https://doi.org/10.1016/j.jhazmat.2022.129412
Received 7 April 2022; Received in revised form 24 May 2022; Accepted 15 June 2022
Available online 20 June 2022

obtained at 2 ppb level. This study demonstrates the potential of UV-assisted ZnO, EGs, and AAO-based capacitance sensor material for rapidly detecting hazardous gaseous light organic molecules at ambient conditions, and the overall approach can be easily expanded to a novel non-invasive monitoring strategy for light and hazardous volatile organic exposures.

1. Introduction

Methanol is a common industrial and laboratory organic solvent that is potentially toxic to the central nervous system of mammals (Skrzydlewska, 2003). It requires careful handling and disposal under applicable local regulatory entities. Ingestion of 30 mL of methanol by a human can cause permanent visual damage, and serum methanol levels of 6.25 mM/L in workers require medical treatment (Nappe, 2021). Particularly, chronic exposure to over 200 ppm methanol gas can cause health-related problems for industrial workers (Gaffney et al., 2008). While specialized testing for serum methanol requires clinical settings, various studies have shown that methanol levels in the blood and exhaled air are related (Ernstgard et al., 2005; Filipiak et al., 2012), which has promoted the use of non-invasive biomarkers for the methanol detection. Most environmental sensors target detection below a time-weighted average of 200 ppm. Detecting such low-level methanol in the atmosphere in a highly sensitive and reliable manner is necessary to develop a real-time and non-invasive health monitoring system. However, sub-ppm-level methanol determination still relies on volumetric gas chromatography (Costa et al., 2022; Zhang et al., 2015a).

Therefore, the highly responsive, good repeatability, and selective detection of ppb-level methanol enabled by a small and cost-efficient sensor system is pivotal for future applications (Jiang et al., 2019; Van Den Broek et al., 2019; Wang et al., 2017). Recent studies on methanol gas sensors have demonstrated small chemical sensors using nanostructured materials with improved detection performance for ppb-detection level methanol (Acharyya et al., 2017; Rong et al., 2022). The response could be enhanced by using nanomaterials operating at moderately high temperatures (80–300 °C). Additionally, simple resistive or capacitive mechanisms minimize the form factor of the entire sensor system (Liu et al., 2011). Specifically, capacitive designs, where a slight change in dielectric properties of the parallel plate-based sensor material surface leads to variations in capacitance, consume less power, and are more stable to small changes at low methanol concentrations.

The class of sensor materials also affects various sensing properties, including operating temperature, detection limit, and response and recovery times. Metal oxide (SnO_2, In_2O_3, Fe_2O_3, etc.) composites have been reported to exhibit superior sensing performances at high temperatures (Bajpai et al., 2012; Kim et al., 2017; Lee et al., 2017; Liu et al., 2021; Zhang et al., 2019). Recently, capacitive methanol gas sensors using metal-organic framework (MOF) materials have been reported (Andres et al., 2020; Homayoonnia and Zeinali, 2016; Hosseini et al., 2016). Although some MOF examples are promising and intriguing under ambient conditions, such as copper(II)-benzene-1,3,5-tricarboxylate (Cu-BTC) (Zeinali et al., 2019), MOF materials generally require high fabrication costs and complex preparation processes, which hinder their widespread deployment. Various quantum dot (QD) materials have also gained attention for use in gas sensors, including ZnSe (Wu et al., 2014), CdSe (Wang et al., 2012), doped QDs, and core-shell QDs (Vasudevan et al., 2015). ZnO QDs applications have been reported for gas sensors, and are primarily used in chemoresistive gas sensors based on oxygen chemisorption, which can be operated at high temperatures (Cho et al., 2022; Forleo et al., 2010; Sinha et al., 2021; Zhang et al., 2021). However, QDs tend to have limited stability due to oxidation, which may result in poor performance of gas sensors. Composite materials, including polymers, titanium carbide (Lee et al., 2017), and lead-based QDs (Zhang et al., 2019) have been proposed as strong alternatives, but they can be toxic or require a complex fabrication process. Operating-wise, methanol sensor has been aimed to be sensible at ambient conditions due to the favored energetics and practical usability, however, economically viable methanol sensors and function at room temperature are still elusive.

This study demonstrated a highly responsive, repeatable, and selective methanol gas sensor enabled by the simple fabrication of porous anodic aluminum oxide (AAO) doped with graphene and zinc oxide (ZnO) QDs. AAO was selected as the base platform because it is cost-effective, nanoporous, has a high affinity for various gas molecules, and has a low dielectric constant of ~10, showing excellent sensing performance (Juhász and Mizsei, 2010; Kim et al., 2009). Exfoliated graphene sheets (EGs) were selected because of their high specific surface area, high chemical stability, and relatively low dielectric constant (Cao et al., 2016; Park et al., 2017; Wisitsoraat et al., 2013). The price of graphene continues to decrease owing to technological advances (Lin et al., 2019), and a small amount of EG addition was found to impose an influential sensing behavior. The sensing performance can be maximized with sufficient carboxyl and hydroxyl groups generated on the edge of the graphene oxide sheets (Kang et al., 2010), which allows the graphene surface to easily adsorb gas molecules. Finally, ZnO QDs are deposited onto the EGs on AAO to endow the sensor surface with high UV-absorbing properties (Kumar et al., 2020; Yan et al., 2019), owing to their wide direct band gap (3.37 eV at the room temperature) with increasing polarization field on the sensor surface. These ZnO QDs exhibit high stability, environmental friendliness, and biosafety (Nazir et al., 2017). The sensor developed in this study exhibited a high methanol response of 2.65% at 100 ppm and 1.73 ppb limit of detection (LOD). This work proposes a promising bottom-up synthetic approach using commercial and well-defined materials to fabricate a highly responsive capacitive gas-sensing device for methanol detection at room temperature, which can be further expanded to the development of practical hazardous VOC sensor applications.

2. Experimental

2.1. Materials

All the reagents were used without further purification or treatment. Graphite foil (0.5 mm, 99.8% and Alfa Aesar), platinum foil (0.5 mm, 99.99%, Sigma-Aldrich), ammonium sulfate ($(NH_4)_2SO_4$, 99.0%, Sigma-Aldrich), zinc acetate dihydrate ($Zn(CH_3COO)_2.2\ H_2O$, 98%, Sigma-Aldrich), N, N-dimethylformamide (C_3H_7NO, 99.9%, Daejung), and a porous AAO template (25 mm diameter, 200 nm pore size, Co, Whatman, Japan) were utilized.

2.2. Synthesis of an exfoliated graphene sheet

The EGs were synthesized using an electrochemical exfoliation process. Graphite and platinum foil were placed in a 0.1 M ammonium sulfate solution with a positive DC potential of 10 V applied to the graphite electrode. The EGs were collected and rinsed several times with deionized water. The as-obtained sample was dispersed in deionized (DI) water by bath sonication, centrifuged at 10,000 rpm for 5 min, and finally into a 50 mL ethanol solution. The supernatant dispersion was carefully separated, and the graphene content in the solution was fixed at 1.6 wt% for further processing.

2.3. Synthesis of ZnO quantum dots

Precursors were formed by dissolving zinc acetate dihydrate powder

(1 wt%) in a precise proportion into an N, N-dimethylformamide (DMF) solution. After precursor solutions had been stirred for 10 min at room temperature, the precursor was heated to 105 °C for 0.5 h, 1 h, 2 h, 3 h, 4 h, 5 h, and 8 h. Colloidal ZnO QDs were formed when the precursor cooled to room temperature. The ZnO QD solution was centrifuged at 10,000 rpm for 5 min and then placed into a 50 mL ethanol solution.

2.4. Design of the gas sensor

The sensor fabrication process was based on a simple dropping method, in which an AAO template was used as an electrically insulating substrate. The fabrication process of the gas sensor is illustrated in Fig. 1 (a). Gold sputtering was used to fabricate electrodes. The electrode was fabricated with a ring shape at the top and a circular shape at the bottom of the AAO template. The electrode was then connected using a copper wire from top to bottom. An ethanol solution containing EGs (0.5 mL/50 mL in ethanol) was deposited on the AAO template, followed by ZnO (0.5 mL/50 mL in ethanol). Finally, the gas sensor was dried at room temperature to evaporate remaining ethanol.

2.5. Sensing system of the methanol gas sensor

The fabrication of the sensing system is illustrated in Fig. 1(b). The gas-sensing performance was evaluated using a computer-controlled system. The fabricated capacitive gas sensor was then placed in a test chamber. The gas concentrations were controlled by changing the ratio of dry air (21% O_2 + 79% N_2) to methanol (i.e. 500 ppm or 10 ppm in dry air as a balanced gas) using mass flow controllers from 100 ppb to 300 ppm at room temperature (25.0 ± 1 °C). The sensor was exposed to different concentrations of methanol gas for 300 s or 1 h, followed by air purging for 300 s or 1 h before the next exposure. Dry air was used as the carrier gas, at a fixed flow rate of 500 sccm. Experiments were performed at an applied voltage of 1.0 V. The adsorption of gas molecules by AAO, EGs/AAO, and EGs-ZnO/AAO causes a change in the sensor capacitance. UV with a wavelength of 275 nm was supplied with 8.0 V power. The detailed sensing process is illustrated in Fig. 2. After stabilization with flowing air, a UV light was turned on when methanol gas began to flow, maximizing the number of adsorption sites to form a polarization field. Desorption was performed as the dry air gas flowed again. The changes in the capacitance of the sensor upon exposure to methanol gas were related only to the change in the dielectric constant of the dielectric material, that is, the EGs-ZnO/AAO gas sensor. The capacitance (C) of the capacitor is expressed by Eq. (1):

$$C = \varepsilon_0 \varepsilon_r A/d \quad (1)$$

Depending on the target gas concentration in the atmosphere, one of the parameters of the distance between the electrodes (d), dielectric constant in vacuum (ε_0), dielectric constant (ε_r), or the area of the electrode (A) must be changed in the capacitive gas sensor. The capacitance sensor response represents the changes in C measured by an inductance–capacitance–resistance (LCR) meter, where the response is defined by Eq. (2), where C_0 and C_g are the capacitance of the sensor in dry air and the concentration of methanol gas, respectively.

$$\text{Response } (\%) = \Delta C/C_0 = (C_g - C_0)/C_0 \times 100 \quad (2)$$

2.6. Characterizations

Surface-enhanced Raman scattering spectra were obtained using a portable Raman system (i-Raman, B&W TEK, USA) equipped with a diode laser emitting light at 532 nm wavelength. High-resolution X-ray photoelectron spectroscopy (XPS) was performed at the Korea Basic Science Institute in Daejeon, Korea. UV–visible absorption spectra were recorded using a UV/visible spectrophotometer (JASCO V-730, METTLER TOLEDO). Room-temperature photoluminescence (PL) spectra were obtained using an excitation laser of 270 nm (LabRAM HR800, Horiba Jobin Yvon Corp., France). The X-ray diffraction (XRD) patterns of the solid were obtained using a D/Max 2200 diffractometer (Rigaku Co., Japan) with Cu Kα radiation (λ = 0.1541 nm) operating at 40 kV and 100 mA in the 2θ range of 10–80° at a scan speed of 4°/min. The morphologies and sizes of the as-obtained samples were observed using transmission electron microscopy (TEM; JEM-2100 F, JEOL, Japan) at 200 kV to obtain high-resolution images. Capacitance–time measurements were performed using an Agilent E4980A LCR meter from 100 Hz to 1 MHz and fixed at 1 V.

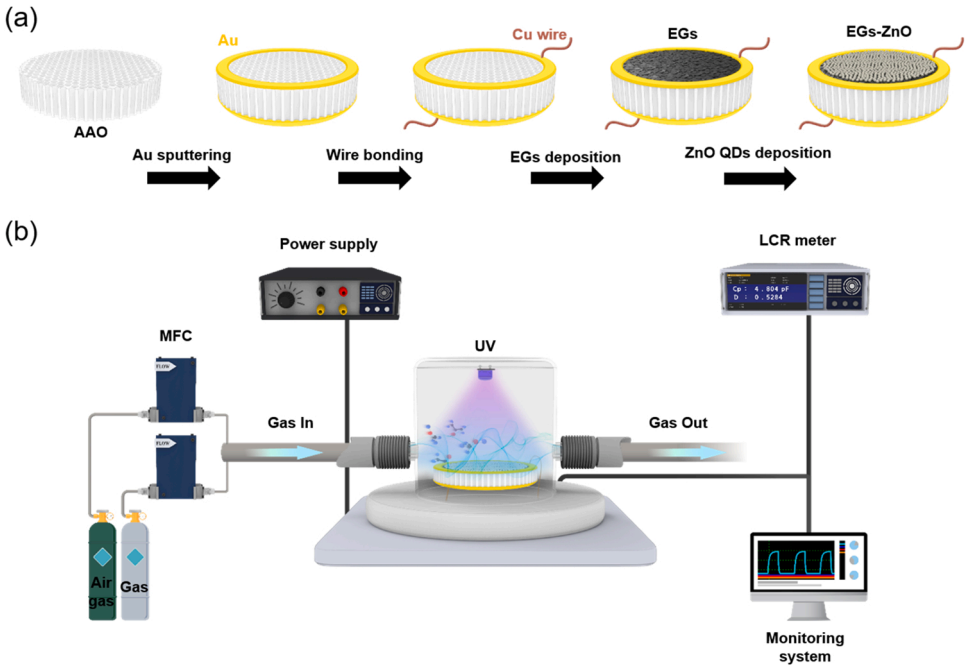

Fig. 1. Schematic diagram of (a) the fabrication procedure of the EGs-ZnO/AAO capacitive gas-sensing unit and (b) gas-sensing experimental setup using UV light.

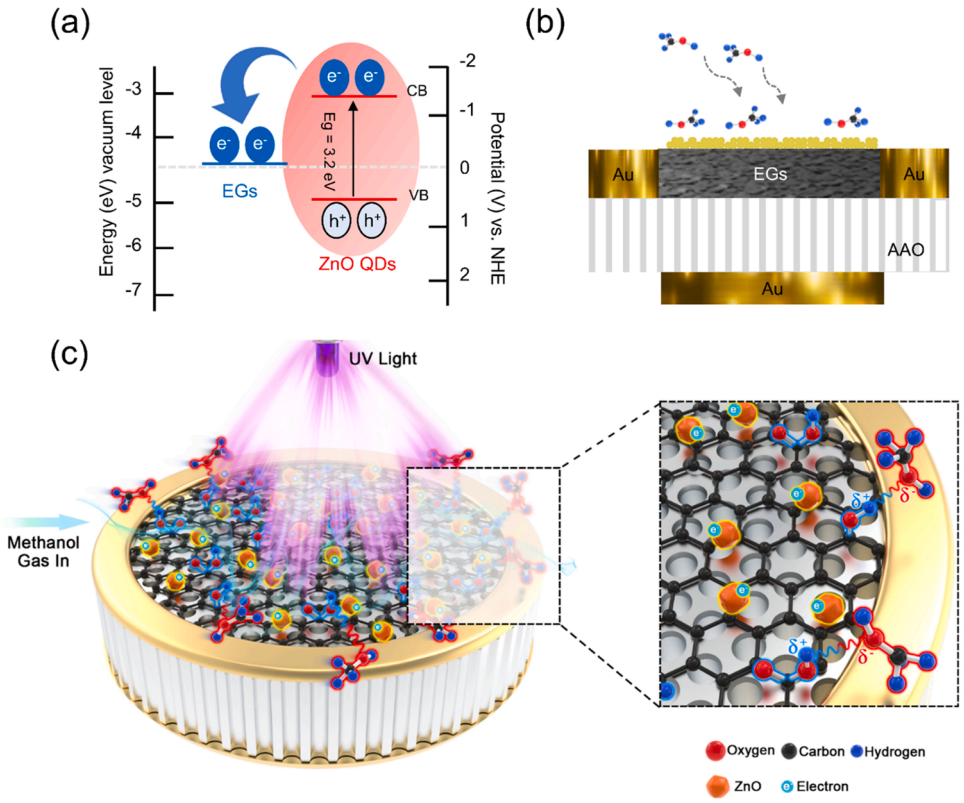

Fig. 2. (a) Schematic diagram of EGs-ZnO QDs band gap, (b) cross-sectional image, and (c) 3D-visualized sensing mechanism of the EGs-ZnO/AAO gas sensor under UV light.

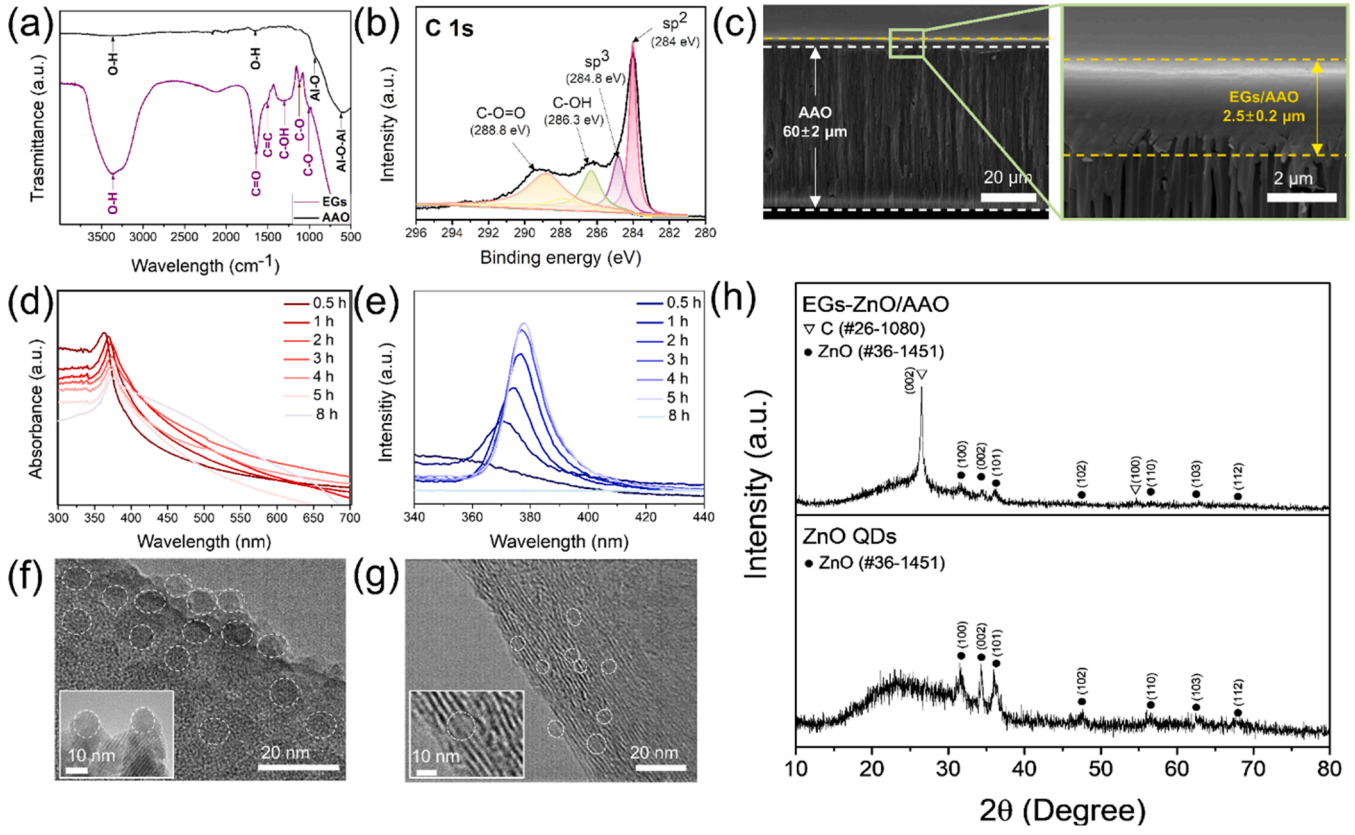

Fig. 3. (a) FT-IR spectrum of AAO and EGs/AAO, (b) XPS spectrum of C 1 s by EGs, (c) SEM image of EGs/AAO, (d) UV–vis of ZnO QDs, and (e) photoluminescence of ZnO QDs, TEM image of (f) ZnO QDs, (g) EGs-ZnO QDs/AAO and (h) XRD pattern of ZnO QDs and EGs-ZnO/AAO gas sensor.

3. Results and discussion

3.1. Sensing mechanism

The structure of the energy levels constructed in the EGs-ZnO/AAO gas sensor under UV light is shown in Fig. 2(a). Based on the relevant band positions of ZnO QDs and EGs, photoinduced electrons are easily transferred from the ZnO QDs conduction band to the EGs. This can efficiently separate the photoinduced electrons and hinder charge recombination in electron transfer processes(Liu et al., 2019; Roy et al., 2013; Xu et al., 2016; Zhang et al., 2015a, 2015b), thus enhancing the response performance of the gas sensor. Fig. 2(b) shows a schematic cross-sectional view of the gas sensor. Compared to the case without UV light, the gas sensor absorbs UV light and increases polarization on the gas sensor surface, inducing a response. The dielectric constant is the measurement of the charge stored inside the material in the presence of an applied electric field and detects the dipole alignment strength. When the EGs-ZnO/AAO gas sensor was exposed to methanol gas molecules, methanol with a dipole moment was adsorbed in greater amounts, attracted by the hydroxyl and carboxyl groups of the EGs defect sites (Panda et al., 2016; Wu et al., 2018). Simultaneously, ZnO QDs reinforce the electric field on the sensor surface, as shown in Fig. 2(c). The sensor was exposed to methanol (32.70) with dielectric constants higher than that of air at room temperature, and the capacitance increased.

3.2. Sensor characterization

The FT-IR spectrum was also used to explore the attachment of functional groups to AAO and EG/AAO, as shown in Fig. 3(a). The peaks at 625 cm^{-1} and 935 cm^{-1} correspond to the Al-oxide stretching vibrations. The large O–H stretching peak at 3433 cm^{-1} indicated an abundance of O–H functional groups (Wu et al., 2016). The sharp peaks at 1389 cm^{-1}, 1050 cm^{-1}, and 1121 cm^{-1} are characteristic of the C–OH and C–O stretching vibrations, respectively (Panda et al., 2016). In addition, the C═O stretching vibration in the carboxyl group was visible at approximately 1647 cm^{-1}. A high-intensity major peak at approximately 1490 cm^{-1} represents the C–partial double bond–C ring stretching vibration. The O–H stretching peak was stronger in EG/AAO than in AAO. There was no peak related to -C in the AAO, but high-intensity peaks were observed in the EGs. Fig. 3(b) shows the XPS spectral characteristics of carbon in the EGs. The C 1 *s* XPS profiles provide useful information on the surface elemental composition and functional groups. The C 1 *s* spectrum indicated four types of carbon bonds, assigned to C–OH, C–O═O, sp^2 C–C bonds, and sp^3 C–O bonds in EGs (Johra et al., 2014). These analyses confirmed the presence of hydroxyl and carboxyl groups at the defect sites of the EGs. The morphologies of EGs/AAO and EGs, characterized using SEM, are shown in Fig. 3(c). The average film thickness of the EGs/AAO was 60 ± 2 μm, whereas the thickness of the EGs was 2.5 ± 0.2 μm. The UV–vis absorption spectra of the ZnO QDs are shown in Fig. 3(d). As the size of the ZnO QDs increased with increasing growth time, the property adsorption peaks for the synthesized ZnO QDs were red-shifted. From the UV–vis results, the band gap values of the ZnO QDs can be determined from the Tauc plot of $(\alpha h\nu)^2$ versus $h\nu$, where α is the absorbance, h is Planck's constant, and ν is the frequency of the photon (Coulter and Birnie, 2018). The properties of ZnO QDs are listed in Table 1. The optical energy bandgap (E_g) decreases from 3.46 eV for ZnO QDs with 0.5 h synthesis time to 3.26 eV with 8 h. All values were close to bulk ZnO (~3.37 eV). The effective mass approximation theoretically describes the increase in the bandgap energy owing to the increased quantum confinement of the electron-hole system in nanoparticles. Eq. (3) shows the relationship between the radius R of spherical nanocrystals and their E_g based on the effective mass model approximation (Brus, 1986):

$$E_{QDs} = E_g \frac{h^2\pi^2}{2R^2}\left(\frac{1}{m_e}+\frac{1}{m_h}\right) - \frac{1.8e^2}{\varepsilon R} \quad (3)$$

where E_g is the bandgap of the bulk material (3.37 eV), h is the reduced Planck's constant, e is the electron charge, ε is the semiconductor dielectric constant, m_e and m_h are the effective masses of electrons and holes, and m_0 is the free electron mass. Using the effective masses of electrons $m_e = 0.26m_0$ and holes $m_h = 0.59m_0$, the radius and diameter of the nanocrystals were calculated. Increasing the synthesis time allowed the average diameter of the ZnO QDs to be tuned from 5.23 nm to 9.45 nm. The PL emission spectra of the ZnO QDs are shown in Fig. 3 (e). As the particle diameter increased, the emission wavelength red-shifted from 370 nm to 378 nm. The intensity of the PL emission increased as the synthesis time of the ZnO QDs increased; however, the intensity of the PL emission did not increase after 8 h. Because the recombination of electrons and holes occurs as it is close to the bulk bandgap. With less than 4 h synthesis time, a small diameter, and a large surface area of the ZnO QDs, particles with more surface defects were formed. Therefore, a synthesis time of less than 4 h correlates with the reduction in the effective luminescent center at the dot surface. The TEM (HRTEM) images of the ZnO QDs and EGs-ZnO/AAO gas sensors in Fig. 3 (f) and (g) show that the ZnO QDs were deposited on the surfaces of the EGs. The average size of the ZnO QDs was determined to be ~ 9 nm. Fig. 3(h) shows the XRD patterns of the independent ZnO QDs and EGs-ZnO/AAO gas sensors. The ZnO QDs exhibited strong diffraction peaks at 2θ = 31.48°, 34.28°, 35.96°, 31.48°, 47.58°, 56.52°, 62.48°, and 67.7°, which were indexed as the (100), (002), (101), (102), (110), (103), and (112) diffraction peaks of the hexagonal phase with the wurtzite crystal structure of ZnO QDs (JDPDS file no. 36–1451). Furthermore, the diffraction peaks of the EGs-ZnO/AAO gas sensor correspond to the characteristic diffraction peak of EGs with a 2θ of 26.5° in the ZnO QDs phase.

Table 1
Properties and nanoparticle sizes of ZnO QDs at different synthesis times.

Synthesis time (h)	Band gap (eV)	Emission peak (nm)	Size (nm)
0.5	3.46	370	5.23
1	3.41	374	7.84
2	3.38	375	8.92
3	3.38	376	8.94
4	3.38	377	8.94
5	3.37	378	9.45
8	3.26	–	–

3.3. Design and stability of the gas sensor with fast response and recovery time

Dielectric materials exhibit frequency-dependent differences in their dielectric properties (Segatin et al., 2020), and the time constants of the electrical dipoles cause this frequency dependence. As shown in Fig. S1, to investigate the performance of the fabricated AAO and EG/AAO gas sensors at different frequencies, the response changes of the sensor in the presence of methanol were measured at various frequencies at a fixed gas concentration of 100 ppm. In Fig. S1(a), although the gas sensor showed a response at a frequency of 1 MHz, it showed a response of approximately 0.004% at 100 ppm AAO. However, 0.108% of that response was for EGs/AAO. EG/AAO gas sensors showed 27 times higher response at 100 ppm compared to AAO, at 1 MHz, as shown in Fig. S1 (b). The response to methanol decreased to less than 1 MHz, as shown in Fig. S1. Because the resonance frequency of the methanol and gas sensors had a minimum of 1 MHz, there was a limit to detecting methanol (Altenberend et al., 2013; Homayoonnia and Zeinali, 2016; Pourteimoor and Haratizadeh, 2017). Therefore, 1 MHz for methanol was identified as the frequency at which the best sensitivities, reflected by capacitance changes, were achieved for a gas concentration of 100 ppm, as shown in Fig. S1(c). Fig. 4 shows real-time capacitance response curves of the horizontal and vertical electrode structures for EGs/AAO gas sensors

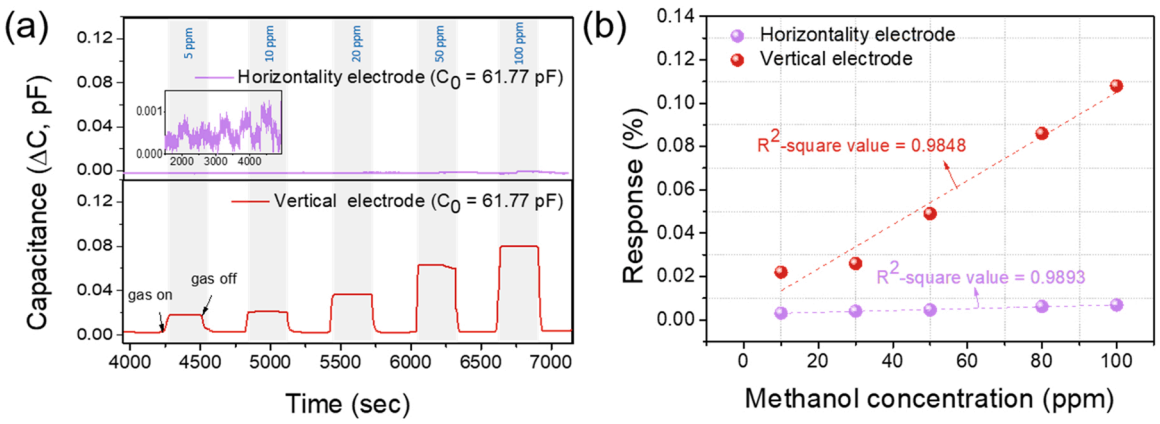

Fig. 4. (a) Real-time capacitance response curves and (b) response of the horizontal electrode structure and vertical electrode structure for EGs/AAO gas sensor with different methanol concentrations of from 10 to 100 ppm at signal frequencies of 1 MHz.

with different methanol concentrations from 10 to 100 ppm at a signal frequency of 1 MHz. A schematic of the EG/AAO gas sensor electrode structure is shown in Fig. S2. The capacitance signal of the gas sensor showed a low signal-to-noise ratio at the horizontal electrode, and the response was 0.006% at 100 ppm methanol. However, the gas sensor capacitance signal showed a high signal-to-noise ratio at the vertical electrode, and high response of 0.108% was obtained with 100 ppm of methanol. The EG/AAO gas sensor exhibits good linearity ($R^2 >$ 0.9848), as shown in Fig. 4(b). The capacitive response in the horizontal configuration was negative and positive in the vertical configuration. In addition, the response was larger than the resistance change, which could be attributed to the capacitance being increased through charge transfer, the dipole moment of the analyses, and the relative changes in the resistance and capacitance increasing with the resistance (Lim et al., 2012).

The experimental capacitance curves of the sensors with gas concentrations ranging from 10 ppm to 300 ppm are shown in Fig. 5(a). The capacitance signals of both sensors steadily increased with increasing methanol concentrations in AAO and EG/AAO. For the AAO and EG/AAO gas sensors, the response reached 0.004% and 0.108% at 100 ppm, showing a 27-fold increase relative to the sensing signal of the AAO gas sensor, as shown in Table 2. The inset of Fig. 5(a) shows that AAO can detect concentrations above 80 ppm and cannot be detected under 50 ppm. Reproducibility is defined as the ability of a sensor to repeat gas concentration measurements under the same conditions. Reversibility is the ability of the sensor to return to its baseline value after the removal of the target gas. Reproducibility is defined as the ability of a sensor to repeat measurements 10 times for gas concentrations at 50 ppm, under the same conditions as those in Fig. 5(b). The same variation in the degree of capacitance was observed during these cycles, indicating the reproducibility of the EG/AAO sensors and their ability to provide reliable results for detecting methanol gas. Fig. 5(c) shows a typical change in the capacitance signal for different methanol concentrations of the AAO and EG/AAO gas sensors. The response directly depended on the gas concentration under all conditions. In addition, the gas sensor exhibited good linearity ($R^2 > 0.9870$ and $R^2 > 0.9953$) for both AAO and EG/AAO, indicating that this material is suitable for the quantitative detection of methanol gas in Fig. 5(d). In Fig. 5(e) and (f), the response

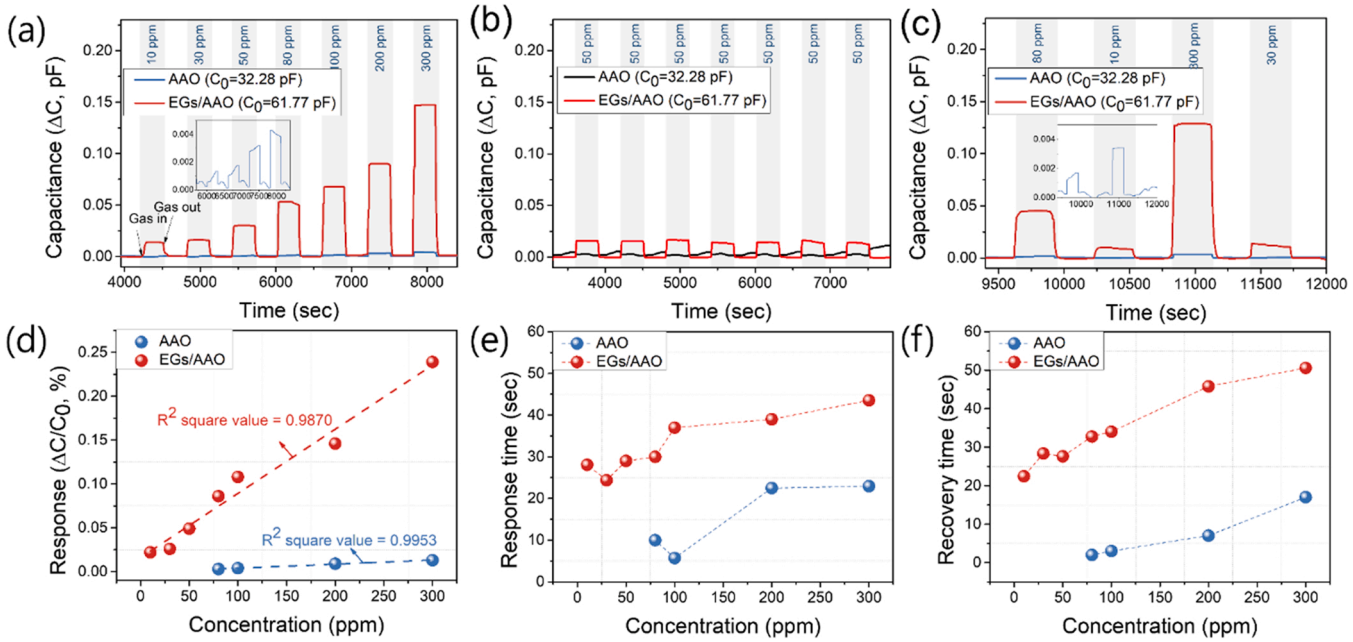

Fig. 5. (a) Real-time capacitance response curves with different methanol concentrations (inset: 80–300 ppm methanol in AAO) (b) 10-times-repeat measurements of curve of gas concentration at 50 ppm under the same conditions (c) change in the capacitance signal at 80–10–300–30 ppm methanol, (d) response, (e) response time and (f) recovery time of AAO and EGs/AAO gas sensor at signal frequencies of 1 MHz.

Table 2
Response changes and calculated response-recovery time versus relative methanol with different concentrations of AAO and EGs/AAO gas sensor at a signal frequency of 1 M Hz.

Concentration (ppm)	AAO			EGs/AAO		
	Response ($\triangle C/C_0$, %)	Response time (sec)	Recovery time (sec)	Response ($\triangle C/C_0$, %)	Response time (sec)	Recovery time (sec)
10	–	–	–	0.022	28.075	22.439
30				0.026	24.380	28.354
50				0.049	29.486	27.623
80	0.003	10.237	2.000	0.086	30.156	32.767
100	0.004	5.710	3.568	0.108	37.256	34.019
200	0.009	22.490	7.256	0.146	39.000	45.803
300	0.013	22.960	17.562	0.239	43.540	50.587

(T_{90}) and recovery time (D_{10}) were calculated for the methanol concentration. The definition of T_{90} and D_{10} are given in the supporting information (Fig. SX). At relatively low methanol concentrations of 10–80 ppm, the T_{90} was delayed (28.07–30.16 s for EGs/AAO); however, as the methanol concentrations increased, the response times decreased (37.26–43.54 s for EGs/AAO). Similar tendencies were observed in the D_{10} of the EG/AAO sensor for methanol gas. The T_{90} and D_{10} values of methanol gas were < 50 s at all concentrations. The calculated responses, T_{90}, and D_{10} are shown in Table 2. Table 3 compares the response and recovery times of previously reported capacitive gas sensors to methanol at room temperature (Chen et al., 2013; Halvaee et al., 2020; Mohammed Mabrook, 2001a; Halvaee Khankahani and Sadegh Beigi, 2018; Tung et al., 2014; Wang et al., 2020). Among the reported capacitive gas sensors, the EG/AAO gas sensor showed a relatively fast response and a short recovery time compared with methanol at 10 ppm and room temperature.

3.4. *Ultra-response in ppb-level and stability of the gas sensor addition to ZnO QDs*

As shown in Fig. 6 and Fig. S3, the change in capacitance of the sensor in the presence of methanol was measured at various frequencies at a fixed gas concentration of 10 ppm to investigate the performance of the fabricated sensors at different frequencies. The EGs/AAO gas sensor without the UV light showed no response below 1 MHz and approximately 0.029% at 1 MHz. The EGs/AAO gas sensor with the UV light exhibited a response from 1 kHz to 1 MHz, with the highest response being 0.316% at 1 MHz. The EGs-ZnO/AAO gas sensors with UV light showed a response from 1 kHz to 1 MHz. In particular, the response was high at 100 kHz, and 1.8740% at 10 ppm. EGs/AAO gas sensors with UV light showed an approximately 11 times higher response at 1 MHz than EGs/AAO without UV light, and EGs-ZnO/AAO with UV light at 100 kHz showed an approximately 65 times higher response than EGs/AAO with UV light at 1 MHz. The absorption of UV light from EGs/AAO is likely to facilitate adsorption as the high polarization field of the gas sensor surfaces resulted in increased capacitance. Because EGs-ZnO/AAO gas sensors have superior UV light absorption compared with EGs/AAO, the enhanced surface polarization enables easier adsorption of methanol, even in the low-frequency range (100 kHz).

Table 3
Literature survey of methanol gas sensing at room temperature.

Materials	Conc. (ppm)	Response time (sec)	Recovery time (sec)	Reference
EGs/AAO	10	28	22	Our study
$Ti_3C_2T_x$/PEDOT:PSS	300	–	–	(Wang et al., 2020)
CoFe Nanoparticle	100	–	–	(Halvaee et al., 2020)
Co_3O_4-intercalated RGO	800	240	360	(Chen et al., 2013)
Fe_2O_3-RGO	1000	140	120	(Tung et al., 2014)
$CoFe_2O_4$ Porous Nanoparticles	100	293	481	(Halvaee Khankahani and Sadegh Beigi, 2018)
TiO_2 Dispersed in PVDF	350	120	360	(Mabrook and Hawkins, 2001)
Au-ZnO QDs Thin Film	10	17	52	(Dey and Sarkar, 2020)
GO/Polyindole Composites	11	1740	1380	(Phasuksom et al., 2020)
Tetratoloylphenyl-porphyrinate Zinc (II)	260	51	92	(Sekrafi et al., 2021)

The experimental capacitance curves of the sensors with gas concentrations ranging from 100 ppb to 800 ppb were obtained at frequencies of 1 MHz with EGs/AAO and 100 kHz with an EG–ZnO/AAO gas sensor. Fig. S4(a) shows a low response with different gas concentrations when the ratio of EGs: ZnO was 1:0.5. The gas sensor with a ratio of EGs: ZnO of 1:1 showed a higher response with different methanol concentrations compared with 1:0.5 of EGs: ZnO QDs. In addition, gas sensors with a ratio of EGs:ZnO of 1:2 showed a high response performance but did not show response properties with different gas concentrations. This phenomenon is confirmed by the linearity corresponding to the gas concentration shown in Fig. 7(a). The EGs: ZnO QDs of the 1:1 gas sensor showed good linearity (R^2 value =0.9751) compared with 1:0.5 (R^2 value =0.8968) and 1:2 (R^2 value =0.0283) of EGs: ZnO QDs ratio. In Fig. S4(b-c), the 1:1 EGs: ZnO QD gas sensor with UV light showed a fast response time (739 s at 800 ppb) and recovery time (110 s at 800 ppb) compared with the 1:0.5 and 1:2 EGs: ZnO QDs sensors. The experimental capacitance curves of the sensors with different gas concentrations ranging from 100 ppb to 800 ppb were obtained at frequencies of 1 MHz and 100 kHz for EGs/AAO without UV light, EGs/AAO with UV light, ZnO/AAO, and EGs-ZnO/AAO with UV light, as shown in Fig. 7(b). The linearity of the gas sensors for methanol gas at concentrations ranging from 100 ppb to 800 ppb is shown in Fig. S5(a). The capacitance curve according to the methanol gas concentration was lower than that of the EGs/AAO gas sensor and EGs-ZnO/AAO with UV light. The response of the gas sensor increased with increasing methanol concentration, showing a high response of 1.2353% for 800 ppb methanol compared with EGs/AAO without UV light and EGs/AAO with UV light. In addition, as shown Fig. S5, the EGs-ZnO/AAO gas sensor exhibited good linearity (R^2 =0.9751) for methanol gas compared with ZnO/AAO (R^2 =0.1602), EGs/AAO without UV light (R^2 =0.8753) and EGs/AAO with UV light (R^2 =0.8902). This indicates that the present material is suitable for the quantitative detection of methanol gas. Furthermore, the low linearity (0.1602 of R^2 value) was confirmed with varying methanol concentrations. This result is attributed to the ZnO QDs which do not directly affect the adsorption of methanol regardless of UV light. We confirmed that ZnO QDs can increase response by maximizing the polarization with UV light only EGs-ZnO QDs/AAO gas sensor. Reproducibility is defined as the ability of a sensor to repeat gas concentration measurements under identical conditions. Reversibility is the ability of the sensor to return to its baseline value after the removal of the target gas. In Fig. 7(c), the stability corresponding to the gas concentration is confirmed through the cross-injection of the gas

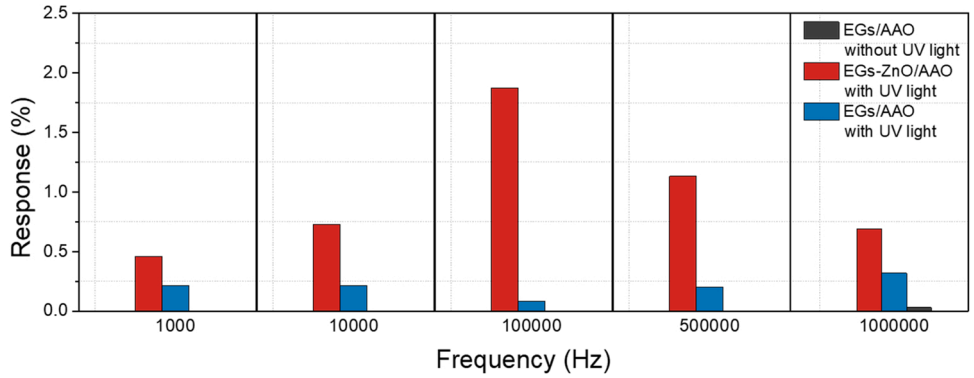

Fig. 6. Response of EGs/AAO and EGs-ZnO/AAO gas sensors at 10 ppm methanol with different frequencies without and with UV light.

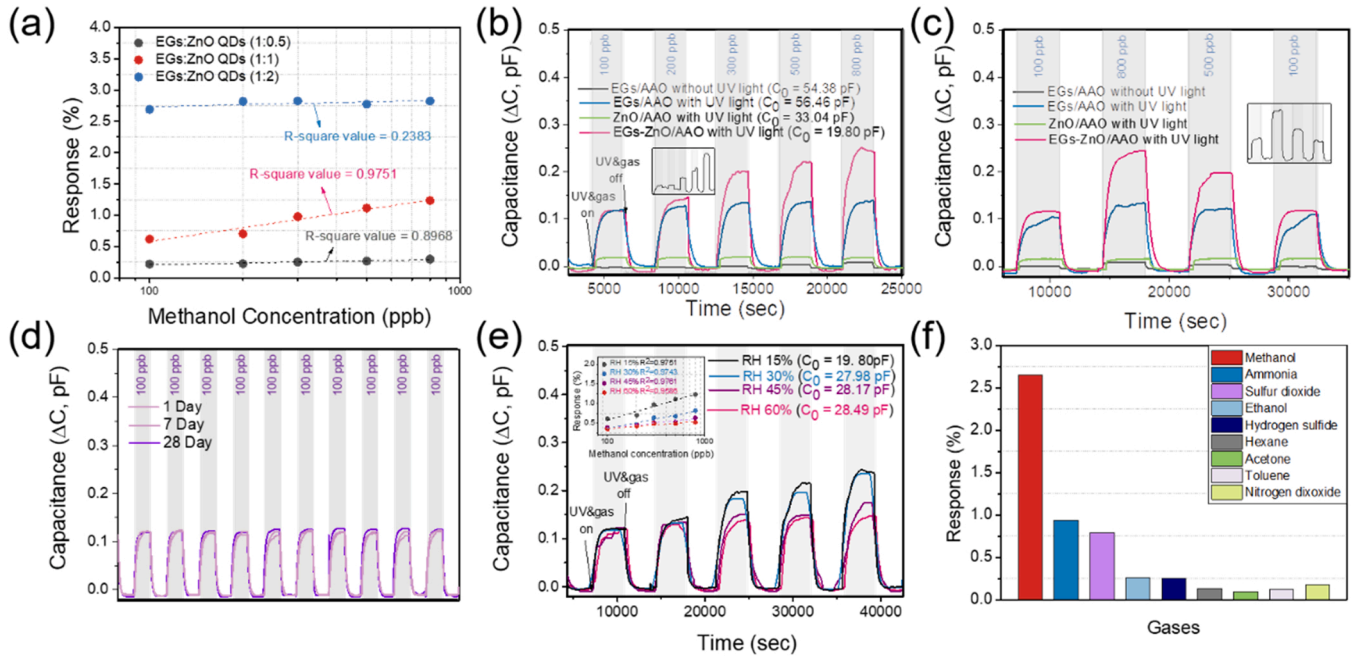

Fig. 7. (a) Response with different methanol gas concentrations of EGs-ZnO QDs (1:0.5, 1:1, and 1:2) gas sensors at a signal frequency of 100 kHz by using a UV light (b) Capacitance response curve change with different methanol gas concentration EGs/AAO, ZnO/AAO and EGs-ZnO/AAO (1:1) gas sensor at a signal frequency of 1 MHz (EGs/AAO) and 100 kHz (ZnO/AAO and EGs-ZnO/AAO) with and without UV light, (c) 100–800–500–100 ppb, (d) capacitance curve of long-term stability with different time (1, 7, 28 days) of EGs-ZnO/AAO with UV light gas sensor fixed at methanol concentrations of 100 ppb. (e) Response of humidity level with different methanol gas concentrations of EGs-ZnO/AAO gas sensor at a signal frequency of 100 kHz (inset: the linearity of response over methanol concentration), and (f) Response of methanol, ammonia, sulfur dioxide, ethanol, hydrogen dioxide, hexane, acetone, toluene, and nitrogen dioxide at fixed 100 ppm for EGs-ZnO/AAO gas sensor at a frequency of 100 kHz with UV light.

concentration of methanol. In Fig. S5(b-c), the response time (T_{90}) and recovery time (D_{10}) were calculated for various methanol concentrations. The detailed response and recovery times versus the relative methanol concentration of the gas sensor are listed in Table 4. Furthermore, the capacitance curve with different methanol concentrations was confirmed by comparing ZnO QDs synthesized at 4 h (EGs-ZnO (4 h)/AAO) and 8 h (EGs-ZnO (8 h)/AAO) and EGs (EGs/AAO) in Fig. S6. This shows the property of the EGs/AAO gas sensor with little effect on ZnO QDs.

Table 5 compares the LODs and responses of previously reported capacitive gas sensors to methanol at room temperature (Andres et al., 2020; Bajpai et al., 2012; Homayoonnia and Zeinali, 2016; Kim et al., 2017; Lee et al., 2017; Mohammed Mabrook, 2001b; Wang et al., 2020). LOD calculation method is discussed in the supporting information (SI. 1.) Among the reported capacitive gas sensors, the EGs-ZnO/AAO gas sensor showed a relatively low LOD and high response to methanol at room temperature. Fig. S7 shows 10 measurement cycles for 10 concentrations of methanol (100 ppb). The same sequence of changes in the degree of capacitance variation was observed during these cycles, indicating the reproducibility of the fabricated sensors and their ability to provide reliable results for methanol gas detection. As shown in Fig. 7 (d), the stability of the sensor was investigated by exposing the sensor to 100 ppb methanol on different days. The sensor retarded the excellent sensing performance without deteriorating it. The humidity-dependent capacitive response was also examined. As shown in Fig. 7(e), the response decreases with increasing relative humidity (RH). Nonetheless, the sensors exhibit good linearity ($R^2 > 0.9586$) at RH 60% and a slightly slow response (Fig. S8(a)), and recovery time (Fig. S7(b)). A variance in the response as a function of humidity is expected because of the high dielectric constant of water. However, the sensor maintained good sensing performance in humid environments. Selectivity is one of the most important parameters for determining the quality of a gas sensor system because it enables the sensor to respond exclusively to a target gas. Fig. 7(f) shows a comparison of the response of the sensor to

Table 4
Response changes and calculated response-recovery time versus varying methanol concentrations of the EGs-ZnO/AAO gas sensor.

	Concentration (ppb)	Response ($\triangle C/C_0$, %)	Response time (sec)	Recovery time (sec)
EGs/AAO without UV light	100	0.001	1.033	6.367
	200	0.002	54.883	6.979
	300	0.009	15.311	7.449
	500	0.013	14.184	12.850
	800	0.022	6.351	12.717
EGs/AAO with UV light	100	0.205	771.000	568.425
	200	0.220	740.000	577.000
	300	0.237	737.230	585.440
	500	0.240	718.980	617.000
	800	0.245	703.130	619.914
EGs-ZnO/AAO with UV light	100	0.618	990.000	519.000
	200	0.703	879.000	222.000
	300	0.976	859.000	129.134
	500	1.114	820.000	113.886
	800	1.2353	739.000	110.000

Table 5
Literature survey of methanol gas-sensing performances at room temperature.

Limit of detection (LOD)	Conc.	Response ($\triangle C/C_0$, %)	Reference
1.73 ppb	100 ppm	2.650	Our study
62 ppm	250 ppm	0.610	(Homayoonnia and Zeinali, 2016)
200 ppm	500 ppm	< 0.001	(Andres et al., 2020)
1 ppm	5000 ppm	1.600	(Bajpai et al., 2012)
9 ppm	100 ppm	0.143	(Lee et al., 2017)
7200 ppm	45000 ppm	1.500	(Kim et al., 2017)
180 ppm	300 ppm	0.700	(Wang et al., 2020)
10 ppm	350 ppm	0.230	(Mohammed Mabrook, 2001b)

methanol in an environment containing multiple gases (e.g., ammonia, sulfur dioxide, ethanol, hydrogen sulfide, hexane, acetone, toluene, and nitrogen dioxide). Methanol exhibited the highest response (2.65%) compared to ammonia, sulfur dioxide, ethanol, hydrogen sulfide, hexane, acetone, toluene, and nitrogen dioxide. The selectivity toward methanol over ethanol is also noteworthy (van den Broek et al., 2019); this indicates the potential and viability of the UV-based approach that can be applied for distinguishing comparable materials. The result demonstrates that the changes in capacitance are highly selective to the methanol under 100 kHz, which is a key advantage of the proposed gas sensor. Based on these results, we concluded that the EGs-ZnO/AAO gas sensor exhibited good selectivity to methanol under our test conditions.

4. Conclusions

We developed a highly responsive sensor for methanol gas using EGs-ZnO/AAO under ultraviolet (UV) light. The EGs-ZnO/AAO gas sensor absorbed UV light, resulting in 56 times increase in response, due to the enhanced polarization on the sensor surface compared with EGs/AAO without UV light. By changing the frequency of UV light, the optimal resonance frequency of methanol was determined to be 100 kHz, with a detected response of 2.65% at 100 ppm. The LOD was estimated to be 1.73 ppb. The humidity-dependent capacitive response was also examined and the sensors exhibited good linearity ($R^2 > 0.9586$) at an RH of 60%. Additionally, the response of the sensor to methanol mixed with multiple hazardous gaseous molecules (e.g., ammonia, sulfur dioxide, ethanol, hydrogen sulfide, hexane, acetone, toluene, and nitrogen dioxide) was compared. This study will help future researchers construct a capacitance sensor with a fast response and low LOD for detecting trace amounts of methanol or other light hazardous gaseous compounds at ambient conditions. The next research steps could involve parametric studies over UV power for energy-efficient sensing, three-phase interface engineering, and fine-tuning of operating conditions toward multimodal use of the sensor to sense various hazardous materials. Further studies should focus on improving the overall sensing performance by ameliorating sensing materials and design structures, as well as combining them with scalable and economical systems to design an IoT-incorporable gas-sensing system suitable for industrial or domestic applications.

CRediT authorship contribution statement

Ji Young Park: Writing – original draft, Conceptualization, Investigation. **Yeonsu Kwak:** Writing – review & editing, Formal analysis. **Hyo-Ryoung Lim:** Resources. **Si-Woo Park:** Resources. **Min Seob Lim:** Validation. **Hong-Baek Cho:** Supervision. **Nosang Vincent Myung:** Writing – review & editing. **Yong-Ho Choa:** Supervision, Funding acquisition, Project administration.

Declaration of Competing Interest

The authors declare that they have no known competing financial interests or personal relationships that could have appeared to influence the work reported in this paper.

Acknowledgment

This work was supported by the Industrial Strategic Technology Development Program (20010460, Developing the Ceramic ALD Precursors with high corrosion resistance and Core Parts of Deposition Etching Equipments for High-Density Semiconductors) and Industrial Strategic Technology Development Program (20010501, Development of Guide Plate for AP Probe Card and MLA Board for DRAM Probe Card Using by AAO Substrate) and funded by the Ministry of Trade, Industry & Energy (MOTIE, Korea).

Environmental implication

Methanol is a widely used organic solvent that can cause blindness (5–10 mL), neurologic sequelae, and even death (> 30 mL) when ingested by humans because of its lethal toxicity. Since the metabolism of methanol to formaldehyde in the liver is potentially harmful to most creatures, waste methanol disposal is able upon the license by the government; the methanol should be discharged after filtration/distillation or incineration. Most environmental sensors target a limited range near a time-weighted average (TWA) of 200 ppm. The solution for detecting low levels of methanol in a hypersensitive, real-time, and reliable manner is increasingly required.

Appendix A. Supporting information

Supplementary data associated with this article can be found in the online version at doi:10.1016/j.jhazmat.2022.129412.

References

Acharyya, D., Acharyya, S., Huang, K., Chung, P., Ho, M., Bhattacharyya, P., 2017. Highly sensitive ppb level methanol sensor by tuning C:O ratio of rGO-TiO_2 nanotube hybrid structure. IEEE Trans. Nanotechnol. 16 (6), 1122–1128. https://doi.org/10.1109/tnano.2017.2764124.

Altenberend, U., Molina-Lopez, F., Oprea, A., Briand, D., Bârsan, N., De Rooij, N.F., Weimar, U., 2013. Towards fully printed capacitive gas sensors on flexible PET substrates based on Ag interdigitated transducers with increased stability. Sens. Actuators B Chem. 187, 280–287. https://doi.org/10.1016/j.snb.2012.11.025.

Andres, M.A., Vijjapu, M.T., Surya, S.G., Shekhah, O., Salama, K.N., Serre, C., Eddaoudi, M., Roubeau, O., Gascon, I., 2020. Methanol and humidity capacitive sensors based on thin films of MOF nanoparticles. ACS Appl. Mater. Interfaces 12 (3), 4155–4162. https://doi.org/10.1021/acsami.9b20763.

Bajpai, R., Motayed, A., Davydov, A.V., Oleshko, V.P., Aluri, G.S., Bertness, K.A., Rao, M. V., Zaghloul, M.E., 2012. UV-assisted alcohol sensing using SnO_2 functionalized GaN nanowire devices. Sens. Actuators B Chem. 171–172, 499–507. https://doi.org/10.1016/j.snb.2012.05.018.

Brus, L., 1986. Electronic wave functions in semiconductor clusters experiment and theory. J. Phys. Chem. 90, 2555–2560.

Cao, F., Zhao, M., Yu, Y., Chen, B., Huang, Y., Yang, J., Cao, X., Lu, Q., Zhang, X., Zhang, Z., Tan, C., Zhang, H., 2016. Synthesis of two-dimensional $CoS_{1.097}$/nitrogen-doped carbon nanocomposites using metal-organic framework nanosheets as precursors for supercapacitor application. J. Am. Chem. Soc. 138 (22), 6924–6927. https://doi.org/10.1021/jacs.6b02540.

Chen, N., Li, X., Wang, X., Yu, J., Wang, J., Tang, Z., Akbar, S.A., 2013. Enhanced room temperature sensing of Co_3O_4-intercalated reduced graphene oxide based gas sensors. Sens. Actuators B Chem. 188, 902–908. https://doi.org/10.1016/j.snb.2013.08.004.

Cho, C.H., Oh, J.Y., Lee, T.I., 2022. Two-dimensional self-assembled network structure of Co_3O_4 quantum-dot-decorated ZnO nanobeads for ppb-level acetone sensors. Mater. Lett. 314. https://doi.org/10.1016/j.matlet.2022.131826.

Costa, B.R.B.D., Haddad, L.P.E., Caleffo Piva Bigão, V.L., Martinis, B.S.D., 2022. Quantifying ethanol in ethanol-based hand sanitizers by headspace gas chromatography with flame ionization detector (HS-GC/FID). J. AOAC Int. 105 (1), 11–18. https://doi.org/10.1093/jaoacint/qsab121.

Coulter, J.B., Birnie, D.P., 2018. Assessing Tauc plot slope quantification: ZnO thin films as a model system. Phys. Status Solidi b 255 (3). https://doi.org/10.1002/pssb.201700393.

Dey, A., Sarkar, S.K., 2020. Room temperature ZnO and Au-ZnO quantum dots thin film gas sensor fabrication for detecting of volatile organic compound gases. IEEE Sens. J. 20 (21), 12602–12609. https://doi.org/10.1109/jsen.2020.3002967.

Ernstgard, L., Shibata, E., Johanson, G., 2005. Uptake and disposition of inhaled methanol vapor in humans. Toxicol. Sci. 88 (1), 30–38. https://doi.org/10.1093/toxsci/kfi281.

Filipiak, W., Ruzsanyi, V., Mochalski, P., Filipiak, A., Bajtarevic, A., Ager, C., Denz, H., Hilbe, W., Jamnig, H., Hackl, M., 2012. Dependence of exhaled breath composition on exogenous factors, smoking habits and exposure to air pollutants. J. Breath. Res. 6 (3), 036008.

Forleo, A., Francioso, L., Capone, S., Siciliano, P., Lommens, P., Hens, Z., 2010. Synthesis and gas sensing properties of ZnO quantum dots. Sens. Actuators B Chem. 146 (1), 111–115. https://doi.org/10.1016/j.snb.2010.02.059.

Gaffney, S., Moody, E., Mckinley, M., Knutsen, J., Madl, A., Paustenbach, D., 2008. Worker exposure to methanol vapors during cleaning of semiconductor wafers in a manufacturing setting. J. Occup. Environ. Hyg. 5 (5), 313–324. https://doi.org/10.1080/15459620801988014.

Halvaee, P., Dehghani, S., Hoghoghifard, S., 2020. Low temperature methanol sensors based on cobalt ferrite nanoparticles, nanorods, and porous nanoparticles. IEEE Sens. J. 20 (8), 4056–4062. https://doi.org/10.1109/jsen.2019.2963456.

Halvaee Khankahani, P., Sadegh Beigi, M., 2018. Room temperature methanol sensor based on ferrite cobalt ($CoFe_2O_4$) porous nanoparticles. J. Electr. Comput. Eng. Innov. 6, 215–222.

Homayoonnia, S., Zeinali, S., 2016. Design and fabrication of capacitive nanosensor based on MOF nanoparticles as sensing layer for VOCs detection. Sens. Actuators B Chem. 237, 776–786. https://doi.org/10.1016/j.snb.2016.06.152.

Hosseini, M.S., Zeinali, S., Sheikhi, M.H., 2016. Fabrication of capacitive sensor based on Cu-BTC (MOF-199) nanoporous film for detection of ethanol and methanol vapors. Sens. Actuators B Chem. 230, 9–16. https://doi.org/10.1016/j.snb.2016.02.008.

Jiang, Y., Ma, J., Lv, J., Ma, H., Xia, H., Wang, J., Yang, C., Xue, M., Li, G., Zhu, N., 2019. Facile wearable vapor/liquid amphibious methanol sensor. ACS Sens. 4 (1), 152–160. https://doi.org/10.1021/acssensors.8b01111.

Johra, F.T., Lee, J.-W., Jung, W.-G., 2014. Facile and safe graphene preparation on solution based platform. J. Ind. Eng. Chem. 20 (5), 2883–2887. https://doi.org/10.1016/j.jiec.2013.11.022.

Juhász, L., Mizsei, J., 2010. A simple humidity sensor with thin film porous alumina and integrated heating. Procedia Eng. 5, 701–704. https://doi.org/10.1016/j.proeng.2010.09.206.

Kang, X., Wang, J., Wu, H., Liu, J., Aksay, I.A., Lin, Y., 2010. A graphene-based electrochemical sensor for sensitive detection of paracetamol. Talanta 81 (3), 754–759. https://doi.org/10.1016/j.talanta.2010.01.009.

Kim, M.G., Alrowais, H., Kim, C., Yeon, P., Ghovanloo, M., Brand, O., 2017. All-soft, battery-free, and wireless chemical sensing platform based on liquid metal for liquid- and gas-phase VOC detection. Lab Chip 17 (13), 2323–2329. https://doi.org/10.1039/c7lc00390k.

Kim, Y., Jung, B., Lee, H., Kim, H., Lee, K., Park, H., 2009. Capacitive humidity sensor design based on anodic aluminum oxide. Sens. Actuators B Chem. 141 (2), 441–446. https://doi.org/10.1016/j.snb.2009.07.007.

Kumar, R., Liu, X., Zhang, J., Kumar, M., 2020. Room-temperature gas sensors under photoactivation: from metal oxides to 2D materials. Nano Micro Lett. 12 (1), 164. https://doi.org/10.1007/s40820-020-00503-4.

Lee, E., VahidMohammadi, A., Prorok, B.C., Yoon, Y.S., Beidaghi, M., Kim, D.J., 2017. Room temperature gas sensing of two-dimensional titanium carbide (MXene). ACS Appl. Mater. Interfaces 9 (42), 37184–37190. https://doi.org/10.1021/acsami.7b11055.

Lim, J.H., Mulchandani, A., Myung, N.V., 2012. Single-walled carbon nanotubes based chemicapacitive sensors. J. Nanosci. Nanotechnol. 12 (2), 1517–1520. https://doi.org/10.1166/jnn.2012.4605.

Lin, L., Peng, H., Liu, Z., 2019. Synthesis challenges for graphene industry. Nat. Mater. 18 (6), 520–524. https://doi.org/10.1038/s41563-019-0341-4.

Liu, J., Sun, F., Zhang, F., Wang, Z., Zhang, R., Wang, C., Qiu, S., 2011. In situ growth of continuous thin metal–organic framework film for capacitive humidity sensing. J. Mater. Chem. 21 (11) https://doi.org/10.1039/c0jm03123b.

Liu, J., Zhang, Y.-H., Bai, Z.-M., Huang, Z.-A., Gao, Y.-K., 2019. Photoelectrocatalytic oxidation of methane into methanol and formic acid over ZnO/graphene/polyaniline catalyst. Chin. Phys. B 28 (4). https://doi.org/10.1088/1674-1056/28/4/048101.

Liu, M., Wang, Z., Song, P., Yang, Z., Wang, Q., 2021. In_2O_3 nanocubes/$Ti_3C_2T_x$ MXene composites for enhanced methanol gas sensing properties at room temperature. Ceram. Int. 47 (16), 23028–23037. https://doi.org/10.1016/j.ceramint.2021.05.016.

Mabrook, M., Hawkins, P., 2001. A rapidly-responding sensor for benzene, methanol and ethanol vapours based on films of titanium dioxide dispersed in a polymer operating at room temperature. Sens. Actuators B Chem. 75 (3), 197–202 https://doi.org/Doi 10.1016/S0925-4005(01)00761-4.

Mohammed Mabrook, P.H., 2001a. A rapidly responding sensor for benzene methanol and ethnaol vapours based on films of titanium dioxide dispersed in a polymer operating at room temperature. Sens. Actuators B Chem. 75, 197–202.

Mohammed Mabrook, P.H., 2001b. A rapidly-responding sensor for benzene, methanol and ethanol vapours based on films of titanium dioxide dispersed in a polymer operating at room temperature. Sens. Actuators B Chem. 75, 197–202.

Nappe., J.V.A.T.M., 2021. Methanol toxicity.

Nazir, G., Khan, M.F., Akhtar, I., Akbar, K., Gautam, P., Noh, H., Seo, Y., Chun, S.-H., Eom, J., 2017. Enhanced photoresponse of ZnO quantum dot-decorated MoS_2 thin films. RSC Adv. 7 (27), 16890–16900. https://doi.org/10.1039/c7ra01222e.

Panda, D., Nandi, A., Datta, S.K., Saha, H., Majumdar, S., 2016. Selective detection of carbon monoxide (CO) gas by reduced graphene oxide (rGO) at room temperature. RSC Adv. 6 (53), 47337–47348. https://doi.org/10.1039/c6ra06058g.

Park, J., Kim, Y.S., Sung, S.J., Kim, T., Park, C.R., 2017. Highly dispersible edge-selectively oxidized graphene with improved electrical performance. Nanoscale 9 (4), 1699–1708. https://doi.org/10.1039/c6nr05902c.

Phasuksom, K., Prissanaroon-Ouajai, W., Sirivat, A., 2020. A highly responsive methanol sensor based on graphene oxide/polyindole composites. RSC Adv. 10 (26), 15206–15220. https://doi.org/10.1039/d0ra00158a.

Pourteimoor, S., Haratizadeh, H., 2017. Performance of a fabricated nanocomposite-based capacitive gas sensor at room temperature. J. Mater. Sci. Mater. Electron. 28 (24), 18529–18534. https://doi.org/10.1007/s10854-017-7800-y.

Rong, Q., Xiao, B., Zeng, J., Yu, R., Zi, B., Zhang, G., Zhu, Z., Zhang, J., Wu, J., Liu, Q., 2022. Pt single atom-induced activation energy and adsorption enhancement for an ultrasensitive ppb-level methanol gas sensor. ACS Sens. 7 (1), 199–206. https://doi.org/10.1021/acssensors.1c01959.

Roy, P., Periasamy, A.P., Liang, C.T., Chang, H.T., 2013. Synthesis of graphene-ZnO-Au nanocomposites for efficient photocatalytic reduction of nitrobenzene. Environ. Sci. Technol. 47 (12), 6688–6695. https://doi.org/10.1021/es400422k.

Segatin, N., Pajk Zontar, T., Poklar Ulrih, N., 2020. Dielectric properties and dipole moment of edible oils subjected to 'Frying' thermal treatment. Foods 9 (7). https://doi.org/10.3390/foods9070900.

Sekrafi, T., Bouricha, B., Denden, Z., Tascu, S., Labidi, A., Nasri, H., Dridi, C., 2021. Development of cost-effective, selective and stable room temperature methanol sensor. IEEE Sens. J. 21 (3), 2589–2596. https://doi.org/10.1109/jsen.2020.3026825.

Sinha, M., Neogi, S., Mahapatra, R., Krishnamurthy, S., Ghosh, R., 2021. Material dependent and temperature driven adsorption switching (p- to n- type) using CNT/ZnO composite-based chemiresistive methanol gas sensor. Sens. Actuators B Chem. 336. https://doi.org/10.1016/j.snb.2021.129729.

Skrzydlewska, E., 2003. Toxicological and metabolic consequences of methanol poisoning. Toxicol. Mech. Methods 13 (4), 277–293. https://doi.org/10.1080/713857189.

Tung, T.T., Castro, M., Pillin, I., Kim, T.Y., Suh, K.S., Feller, J.-F., 2014. Graphene–Fe_3O_4/PIL–PEDOT for the design of sensitive and stable quantum chemo-resistive VOC sensors. Carbon 74, 104–112. https://doi.org/10.1016/j.carbon.2014.03.009.

Van Den Broek, J., Abegg, S., Pratsinis, S.E., Güntner, A.T., 2019. Highly selective detection of methanol over ethanol by a handheld gas sensor. Nat. Commun. 10 (1) https://doi.org/10.1038/s41467-019-12223-4.

Vasudevan, D., Gaddam, R.R., Trinchi, A., Cole, I., 2015. Core–shell quantum dots: properties and applications. J. Alloy. Compd. 636, 395–404. https://doi.org/10.1016/j.jallcom.2015.02.102.

Wang, C., Kou, X., Xie, N., Guo, L., Sun, Y., Chuai, X., Ma, J., Sun, P., Wang, Y., Lu, G., 2017. Detection of methanol with fast response by monodispersed indium tungsten oxide ellipsoidal nanospheres. ACS Sens. 2 (5), 648–654. https://doi.org/10.1021/acssensors.7b00028.

Wang, T., Zhang, S., Mao, C., Song, J., Niu, H., Jin, B., Tian, Y., 2012. Enhanced electrochemiluminescence of CdSe quantum dots composited with graphene oxide and chitosan for sensitive sensor. Biosens. Bioelectron. 31 (1), 369–375. https://doi.org/10.1016/j.bios.2011.10.048.

Wang, X., Sun, K., Li, K., Li, X., Gogotsi, Y., 2020. Ti_3C_2T /PEDOT:PSS hybrid materials for room-temperature methanol sensor. Chin. Chem. Lett. 31 (4), 1018–1021. https://doi.org/10.1016/j.cclet.2019.11.031.

Wisitsoraat, A., Pakapongpan, S., Sriprachuabwong, C., Phokharatkul, D., Sritongkham, P., Lomas, T., Tuantranont, A., 2013. Graphene–PEDOT:PSS on screen printed carbon electrode for enzymatic biosensing. J. Electroanal. Chem. 704, 208–213. https://doi.org/10.1016/j.jelechem.2013.07.012.

Wu, D., Chen, Z., Huang, G., Liu, X., 2014. ZnSe quantum dots based fluorescence sensors for Cu^{2+} ions. Sens. Actuators A Phys. 205, 72–78. https://doi.org/10.1016/j.sna.2013.10.020.

Wu, J., Tao, K., Zhang, J., Guo, Y., Miao, J., Norford, L.K., 2016. Chemically functionalized 3D graphene hydrogel for high performance gas sensing. J. Mater. Chem. A 4 (21), 8130–8140. https://doi.org/10.1039/c6ta01426g.

Wu, J., Feng, S., Li, Z., Tao, K., Chu, J., Miao, J., Norford, L.K., 2018. Boosted sensitivity of graphene gas sensor via nanoporous thin film structures. Sens. Actuators B Chem. 255, 1805–1813. https://doi.org/10.1016/j.snb.2017.08.202.

Xu, J., Cui, Y., Han, Y., Hao, M., Zhang, X., 2016. ZnO–graphene composites with high photocatalytic activities under visible light. RSC Adv. 6 (99), 96778–96784. https://doi.org/10.1039/c6ra19622e.

Yan, X., Wu, Y., Li, R., Shi, C., Moro, R., Ma, Y., Ma, L., 2019. High-performance UV-assisted NO_2 sensor based on chemical vapor deposition graphene at room temperature. ACS Omega 4 (10), 14179–14187. https://doi.org/10.1021/acsomega.9b00935.

Zeinali, S., Homayoonnia, S., Homayoonnia, G., 2019. Comparative investigation of interdigitated and parallel-plate capacitive gas sensors based on Cu-BTC nanoparticles for selective detection of polar and apolar VOCs indoors. Sens. Actuators B Chem. 278, 153–164. https://doi.org/10.1016/j.snb.2018.07.006.

Zhang, C.-Y., Lin, N.-B., Chai, X.-S., Zhong-Li, Barnes, D.G., 2015. A rapid method for simultaneously determining ethanol and methanol content in wines by full evaporation headspace gas chromatography. Food Chem. 183, 169–172. https://doi.org/10.1016/j.foodchem.2015.03.048.

Zhang, S., Chen, H.S., Matras-Postolek, K., Yang, P., 2015. ZnO nanoflowers with single crystal structure towards enhanced gas sensing and photocatalysis. Phys. Chem. Chem. Phys. 17 (45), 30300–30306. https://doi.org/10.1039/c5cp04860e.

Zhang, Y., Pan, W., Dong, G., Zhang, D., 2019. A high-performance room temperature methanol gas sensor based on alpha-iron oxide/polyaniline/PbS quantum dots nanofilm. J. Mater. Sci. Mater. Electron. 30 (19), 17907–17915. https://doi.org/10.1007/s10854-019-02143-w.

Zhang, Y.-H., Wang, C.-N., Yue, L.-J., Chen, J.-L., Gong, F.-L., Fang, S.-M., 2021. Nitrogen-doped graphene quantum dot decorated ultra-thin ZnO nanosheets for NO_2 sensing at low temperatures. Phys. E Low Dimens. Syst. Nanostruct. 133. https://doi.org/10.1016/j.physe.2021.114807.